THE JOURNAL OF PHYSICAL CHEMISTRY Letters

pubs.acs.org/JPCL Letter

Accurate Neural Network Representation of the Ab Initio Determined Spin−Orbit Interaction in the Diabatic Representation Including the Effects of Conical Intersections

Yafu Guan* and David R. Yarkony*

Cite This: J. Phys. Chem. Lett. 2020, 11, 1848−1858 Read Online

ACCESS | Metrics & More | Article Recommendations | Supporting Information

ABSTRACT: A method for fitting ab initio determined spin−orbit coupling interactions, in the Breit−Pauli approximation, based on quasidiabatic representations using neural network fits is reported. The algorithm generalizes our recently reported neural network approach for representing the dipole interaction. The S_0, S_1, and T_1 states of formaldehyde are used as an example. First, the two singlet states S_0 and S_1 are diabatized with a modified Boys Localization diabatization method. Second, the spin−orbit coupling between singlet and triplet states is transformed to the diabatic representation. This removes the discontinuities in the adiabatic representation. The diabatized spin−orbit couplings are then fit with smooth neural network functions. The analytic representation of spin−orbit coupling interactions in a diabatic basis by neural networks will make accurate full-dimensional quantum dynamical treatment of both internal conversion and intersystem crossing possible, which will help us to gain better understanding of both processes.

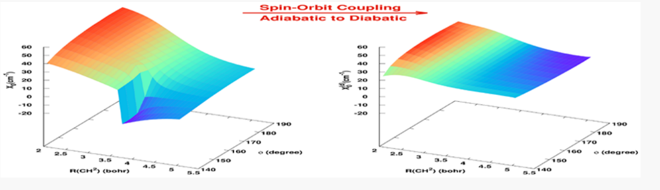

The competition between internal conversion and intersystem crossing is a topic of considerable current interest.[1−4] Here internal conversion refers to spin conserving, conical intersection induced nonadiabaticity, and intersystem crossing refers to spin changing, spin−orbit coupling (SOC) induced nonadiabaticity. To study this competition, a Hamiltonian that treats both processes in an even handed manner is required.

There are two ways to construct a Hamiltonian that treats both processes: the on-the-fly approach in which at each time step the available electronic wave functions determine all the electronic structure data (ESD) needed at that time step;[3,4] and the fit-coupled diabatic state representation approach, in which the energy, energy gradient, and derivative couplings are provided from an analytic coupled diabatic state representation fit to the adiabatic ab initio ESD. The relative merits of these two approaches have been discussed in the literature.[5−7] Treatment of nonadiabatic dynamics may also require spin−orbit or dipole interactions. Incorporating these interactions is straightforward for the on-the-fly approach, since the wave functions are available at each time step. However, for the fit diabatic representation approach, to incorporate these terms, new functional forms and fitting approaches must be devised to account for the different properties of the additional terms. This extra effort is justified owing to the high quality of the ab initio data that can be used in the fit diabatic state approach. Indeed, as the recent numerical studies of intersystem crossing in thioformaldehyde by Mai et al. have demonstrated,[8] the best option for ab initio methods for excited-state dynamics studies is correlated multireference methods, as these methods can provide the correct description of the potential energy surfaces (PESs) and the couplings between them over a wide range of nuclear coordinates. However, due to their high computational cost, these methods are not practical for on-the-fly methods even for small systems. Thus, when high accuracy is required, fit representations are essential. This work addresses this issue by developing a neural network (NN) representation of the spin−orbit interaction within a diabatic framework appropriate for nonadiabatic dynamics based on the eigenvectors of the spin-free nonrelativistic Hamiltonian $\hat{H}_{SF}$. In this regard, previously, Eisfeld, Manthe, and co-workers[9,10] have studied the reaction dynamics of vibronically and spin−orbit-coupled $F(^2P) + CH_4$ using carefully constructed diabatic representations.

Molecular properties or interactions to be fit by analytic functional forms must be smooth and continuous functions of nuclear coordinates. In the adiabatic representation, when it comes to nonadiabatic processes involving conical intersections of electronic states, molecular properties/interactions will exhibit discontinuities, which makes them unsuitable for fitting. However, when transformed to an appropriate diabatic representation, the discontinuities at conical intersections disappear, rendering molecular properties/interactions smooth functions of nuclear coordinates, which eventually can be fit. For polyatomic molecules, rigorous diabatic representations do not

Received: January 8, 2020
Accepted: February 16, 2020
Published: February 17, 2020

exist,[11−13] hence the more precise name is *quasidiabatic*. However, the attribute *quasi* will be omitted below except as needed for emphasis.

The idea of fitting diabatized molecular properties/interactions has been successfully demonstrated in our recent work, in which the diabatized electric dipole and transition dipole moments of the $1,2^1A$ states of ammonia were represented by smooth artificial NN functions.[7] The combination of an accurate derivative-coupling-based diabatization and machine-learning tools contributed greatly to the success of that work. The accurate diabatic representation for $1,2^1A$ states of ammonia was constructed using a derivative-coupling-based diabatization procedure proposed by Zhu and Yarkony (ZY),[6,14−16] in which the ab initio ESD including energies, energy gradients, and derivative couplings are simultaneously fit and diabatized to generate a robust and accurate quasidiabatic representation. Its accuracy has been not only measured by small residual derivative couplings but also demonstrated by excellent agreement with experimentally measured dynamical attributes in the photodissociation of ammonia.[17−20] One potential problem in fitting these matrix elements is the arbitrary sign of the interstate matrix elements. In the previous work, we showed how the arbitrariness in the sign of transition dipole moments could be removed by a cluster growing algorithm[21] with Gaussian process regression (GPR).[22] The diabatized dipole and transition dipole moments were then accurately represented by smooth and flexible artificial NN functions.

Motivated by the success of fitting diabatized dipole and transition dipole moments, in this work, we apply this method to fit spin−orbit coupling (SOC) in a diabatic representation. This will enable an accurate and unified description for both internal conversion and intersystem crossing. This work relies on NN techniques and wave-function-based, as opposed to molecular-orbital-based, diabatizations. It is distinct from previous work in the area, which includes the effective relativistic coupling by asymptotic representation method of Eisfeld et. al,[23] the model space fitting methods of Zeng[24] and of Köppel,[25] and other machine-learning-based approaches.[26−29] The result of our fit can be combined with our NN-based representation of the diabatic potential energy matrix[30−32] to provide the equivalent of wave-function-based input to standard nonadiabatic quantum[2] or surface hopping[3,4,33] dynamics codes.

The photodissociation of formaldehyde will provide an ideal test for our method.[34−43] Photoexcitation of formaldehyde from singlet ground electronic-state S_0 to the first singlet excited-state $S_1(n-\pi^*)$ can lead to both radical dissociation with products H + HCO and molecular dissociation with products H_2 + CO on the ground state. Both dissociations can be explained by internal conversion through either a conical intersection between S_0 and S_1 or radiationless decay from S_1 to S_0. Population in the first triplet excited-state T_1 can also accumulate through intersystem crossing between S_1 and T_1, which leads to radical dissociation on T_1. Through an accessible T_1/S_0 crossing, products on S_0 can also be obtained. To fully investigate the competition between internal conversion and intersystem crossing in the dissociation of formaldehyde, an accurate global and unified description for all three states and the couplings between them is necessary.

The total Hamiltonian $\hat{H}$ used to describe both internal conversion and intersystem crossing will be

$$\hat{H} = \hat{H}_{SF} + \hat{H}_{SO} \quad (1)$$

where $\hat{H}_{SF}$ is the electrostatic spin-free part, also known as the spin-free Born−Oppenheimer Hamiltonian, and $\hat{H}_{SO}$ is the SOC term, here in the Breit−Pauli approximation.[44,45] The $\hat{H}_{SF}$ eigenstates $|i, S, M_S\rangle = \Psi_i^{(a),S,M_S}(\mathbf{r};\mathbf{R})$, where $M_S = -S, -S+1, ..., S-1, S$, $\mathbf{r}$ are the electronic coordinates, and $\mathbf{R}$ is nuclear coordinates, are also eigenstates of $\hat{S}^2$ and $\hat{S}_z$. They are normally called adiabatic states. The eigenvalues of adiabatic-states $E_i^{(a)}(\mathbf{R})$ are the adiabatic PESs. In the case of formaldehyde, S_0, S_1, and T_1 are the adiabatic states of interest. S_0 and S_1 are singlet states with $S = 0$, and T_1 is a triplet state with $S = 1$. It is important to note that T_1 is threefold degenerate in the absence of spin−orbit coupling, which includes the states $|T_1, M_S = -1\rangle$, $|T_1, M_S = 0\rangle$, and $|T_1, M_S = 1\rangle$. S_0, S_1, and T_1 form the adiabatic basis for formaldehyde, and the corresponding representation is the adiabatic representation. S_0 and S_1 are coupled through derivative couplings, which are singular where potential energy surfaces for S_0 and S_1 intersect conically. This singularity also leads to discontinuities in molecular properties/interactions. Therefore, the SOCs between the two singlet states and the triplet state will exhibit discontinuities at the conical intersections between S_0 and S_1.

The way to eliminate this singularity is to transform to a diabatic basis. For the two singlet states, the adiabatic basis and diabatic basis are connected with each other through an orthogonal transformation

$$\begin{pmatrix} |S_0^{(d)}\rangle \\ |S_1^{(d)}\rangle \end{pmatrix} = \begin{pmatrix} \cos\theta & -\sin\theta \\ \sin\theta & \cos\theta \end{pmatrix} \begin{pmatrix} |S_0\rangle \\ |S_1\rangle \end{pmatrix} \quad (2)$$

where $\theta(\mathbf{R})$ is the rotation angle that defines the adiabatic to diabatic (AtD) transformation. In the diabatic basis or in the diabatic representation, the singular derivative couplings are removed, and the residual derivative couplings are negligible. The discontinuities in molecular properties/interactions will also disappear.[7,46] Since T_1 does not interact with S_0 or S_1 through derivative couplings, $S_0^{(d)}$, $S_1^{(d)}$, and T_1 will form a diabatic basis for formaldehyde. According to eq 2, the SOCs between $S_0^{(d)}$, $S_1^{(d)}$, and T_1 will be linear combinations of those in the adiabatic representation

$$\begin{aligned} \langle S_0^{(d)}|\hat{H}_{SO}|T_1, M_S\rangle_{\mathbf{r}} &= \langle S_0|\hat{H}_{SO}|T_1, M_S\rangle_{\mathbf{r}}\cos\theta - \langle S_1|\hat{H}_{SO}|T_1, M_S\rangle_{\mathbf{r}}\sin\theta \\ \langle S_1^{(d)}|\hat{H}_{SO}|T_1, M_S\rangle_{\mathbf{r}} &= \langle S_0|\hat{H}_{SO}|T_1, M_S\rangle_{\mathbf{r}}\sin\theta + \langle S_1|\hat{H}_{SO}|T_1, M_S\rangle_{\mathbf{r}}\cos\theta \end{aligned} \quad (3)$$

where $M_S = 0, \pm 1$.

In the adiabatic representation, the elements of the Hamiltonian matrix, $\mathbf{H}^{(a)}$, for formaldehyde are listed in Table 1. $|T_1, -\rangle$, $|T_1, +\rangle$, and $|T_1, 0\rangle$ are time-reversal-symmetry-adapted[47] triplet states, in which the SOC matrix elements are real, since the spin−orbit coupling operator is invariant under time reversal, i.e., X_i, Y_i, and Z_i ($i = 0, 1$) are real numbers. The transformation properties of X_i, Y_i, and Z_i with respect to rotation are the same as those of the angular momentum operator $\hat{L}_x$, $\hat{L}_y$, and $\hat{L}_z$. For more details about SOC in formaldehyde, please see the Supporting Information. Using eqs

Table 1. Matrix Elements of $\mathbf{H}^{(a)}$ for Formaldehyde

$\hat{H}$	$\|S_0\rangle$	$\|S_1\rangle$	$\|T_1, -\rangle$	$\|T_1, +\rangle$	$\|T_1, 0\rangle$
$\langle S_0\|$	$E(S_0)$	0	X_0	Y_0	Z_0
$\langle S_1\|$	0	$E(S_1)$	X_1	Y_1	Z_1
$\langle T_1, -\|$	X_0	X_1	$E(T_1)$	0	0
$\langle T_1, +\|$	Y_0	Y_1	0	$E(T_1)$	0
$\langle T_1, 0\|$	Z_0	Z_1	0	0	$E(T_1)$

https://dx.doi.org/10.1021/acs.jpclett.0c00074
J. Phys. Chem. Lett. 2020, 11, 1848−1858

Table 2. Matrix Elements of $\mathbf{H}^{(d)}$ for Formaldehyde

$\hat{H}$	$\lvert S_0^{(d)}\rangle$	$\lvert S_1^{(d)}\rangle$	$\lvert T_1, -\rangle$	$\lvert T_1, +\rangle$	$\lvert T_1, 0\rangle$
$\langle S_0^{(d)}\rvert$	$E(S_0)\cos^2\theta + E(S_1)\sin^2\theta$	$[E(S_0) - E(S_1)]\cos\theta\sin\theta$	$X_0\cos\theta - X_1\sin\theta$	$Y_0\cos\theta - Y_1\sin\theta$	$Z_0\cos\theta - Z_1\sin\theta$
$\langle S_1^{(d)}\rvert$	$[E(S_0) - E(S_1)]\cos\theta\sin\theta$	$E(S_0)\sin^2\theta + E(S_1)\cos^2\theta$	$X_0\sin\theta + X_1\cos\theta$	$Y_0\sin\theta + Y_1\cos\theta$	$Z_0\sin\theta + Z_1\cos\theta$
$\langle T_1, -\rvert$	$X_0\cos\theta - X_1\sin\theta$	$X_0\sin\theta + X_1\cos\theta$	$E(T_1)$	0	0
$\langle T_1, +\rvert$	$Y_0\cos\theta - Y_1\sin\theta$	$Y_0\sin\theta + Y_1\cos\theta$	0	$E(T_1)$	0
$\langle T_1, 0\rvert$	$Z_0\cos\theta - Z_1\sin\theta$	$Z_0\sin\theta + Z_1\cos\theta$	0	0	$E(T_1)$

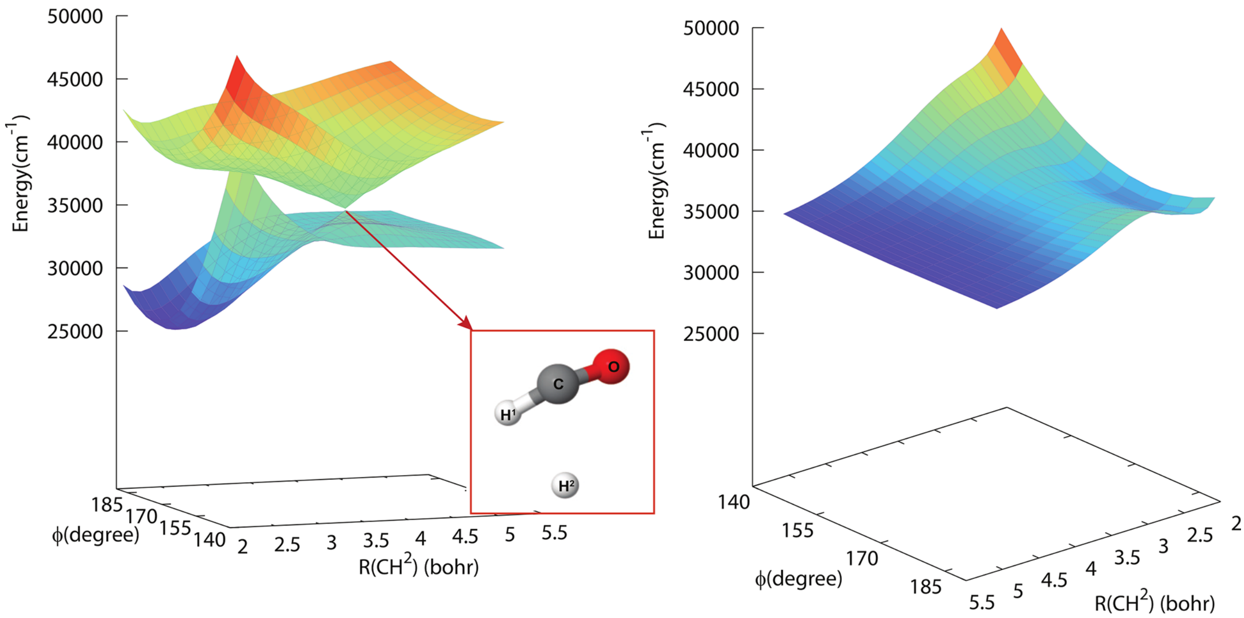

Figure 1. Adiabatic potential energy surfaces for S_0, S_1 (left panel), and T_1 (right panel) in the two-dimensional space. The inset pictures the minimum energy conical intersection (MEX) between S_0 and S_1, where $R(\mathrm{CO}) = 2.238$ bohr, $R(\mathrm{CH}^1) = 2.076$ bohr, $R(\mathrm{CH}^2) = 3.692$ bohr, $\angle \mathrm{H}^1\mathrm{CH}^2 = 65.45°$, $\angle \mathrm{H}^1\mathrm{CO} = 139.04°$, and $\angle \mathrm{H}^2\mathrm{CO} = 107.84°$.

2 and 3, the elements of $\mathbf{H}^{(d)}$, the diabatic representation for formaldehyde, can be obtained and are shown in Table 2.

As noted above, the key to obtaining smooth and continuous diabatized molecular properties/interactions is a proper diabatization method that can remove the singularities in derivative couplings at conical intersections. In this work, a diabatization scheme distinct from that used in the ammonia work described above, a generalized form of the property-based Boys localization (BL) diabatization,[48] is employed. The molecular property used in the BL diabatization is the electric dipole moment. For the diabatization of ith and jth adiabatic electronic states, the rotation angle that defines the AtD transformation satisfies following condition

$$\tan 4\theta_{ij} = \frac{2\mathbf{G}_{i,j}^{(a)}\cdot\mathbf{O}_{i,j}^{(a)}}{\left\|\mathbf{G}_{i,j}^{(a)}\right\|^2 - \left\|\mathbf{O}_{i,j}^{(a)}\right\|^2} \tag{4}$$

where $\mathbf{G}_{i,j}^{(a)} = 1/2(\boldsymbol{\mu}_i^{(a)} - \boldsymbol{\mu}_j^{(a)})$, and $\mathbf{O}_{i,j}^{(a)} = \boldsymbol{\mu}_{ij}^{(a)}.\boldsymbol{\mu}_{ij}^{(a)}$ is the transition dipole moment between the ith and jth states, and $\boldsymbol{\mu}_i^{(a)}$ and $\boldsymbol{\mu}_j^{(a)}$ are the dipole moments of ith and jth states, respectively. BL diabatization can remove singular derivative couplings at conical intersections. However, it also creates erroneous diabolical singularities where actual derivative couplings are finite.[49−52] These diabolical singularities can be removed by introducing a simple modification of eq 4, giving

$$\tan 4\theta_{ij} = \frac{2\mathbf{G}_{i,j}^{(a)}\cdot\mathbf{O}_{i,j}^{(a)}}{\left\|\mathbf{G}_{i,j}^{(a)}\right\|^2 + \frac{w^2}{4}(E_i^{(a)} - E_j^{(a)})^2 - \left\|\mathbf{O}_{i,j}^{(a)}\right\|^2} \tag{5}$$

where w is an adjustable parameter.[50]

Apart from the singularity in derivative coupling, a conical intersection also produces the geometric phase effect.[53−59] When moving along a closed path surrounding the conical intersection, the real adiabatic electronic wave functions will exhibit a sign change, making adiabatic electronic wave functions double-valued. Correspondingly, in a diabatization, the rotation angle will change by π. Considering that $H_{11}^{(d)}$, $H_{12}^{(d)}$, and $H_{22}^{(d)}$ are all periodic functions of the rotation angle with a period of π, they will remain single-valued despite the π change in rotation angle. Therefore, the value of θ_{ij} that satisfies eq 5 should cover a range of π. Let $n = 2\mathbf{G}_{i,j}^{(a)}\cdot\mathbf{O}_{i,j}^{(a)}$ and $d = \|\mathbf{G}_{i,j}^{(a)}\|^2 + \frac{w^2}{4}(E_i^{(a)} - E_j^{(a)})^2 - \|\mathbf{O}_{i,j}^{(a)}\|^2$, θ_{ij} can be obtained through

$$\theta_{ij} = \frac{\mathrm{atan2}(n, d) + k\pi}{4} \tag{6}$$

where the two-argument inverse tangent function atan2(y, x) is used, and $k = 0, \pm 1$. It is easy to show that eq 6 satisfies eq 5 and $\theta_{i,j} \in \left(-\frac{\pi}{2}, \frac{\pi}{2}\right)$, which is a range of π. To obtain the correct θ_{ij}, the sign of transition dipole moment $\boldsymbol{\mu}_{ij}$, which is arbitrary due to the arbitrary phases of electronic wave functions in ab initio calculations, and the value of k have to be (manually) adjusted.

https://dx.doi.org/10.1021/acs.jpclett.0c00074
J. Phys. Chem. Lett. 2020, 11, 1848−1858

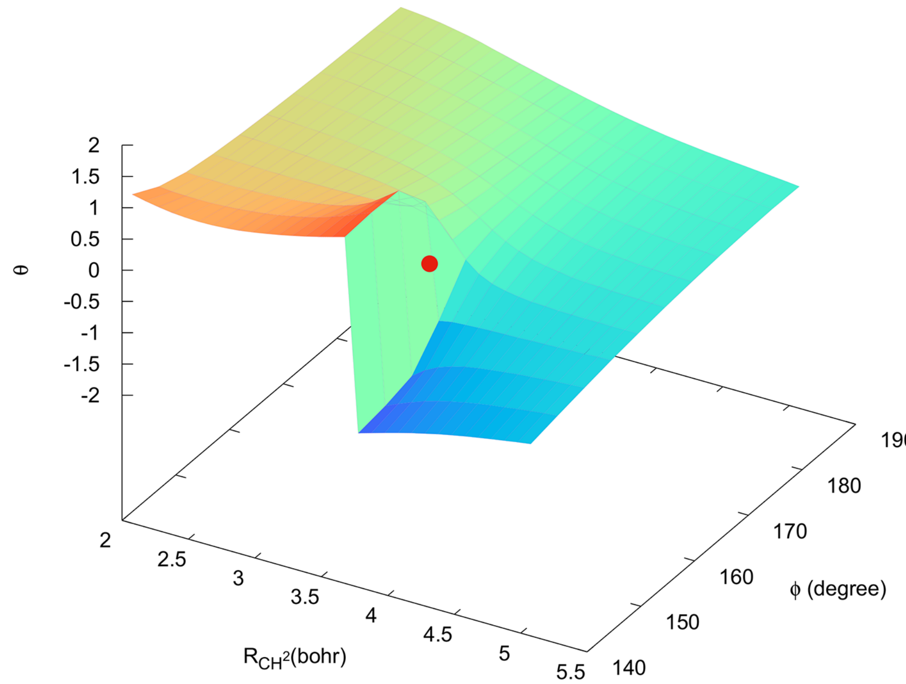

Figure 2. Rotation angle θ from modified BL diabatization (w = 8 au) in the two-dimensional space. The MEX is marked as a red dot.

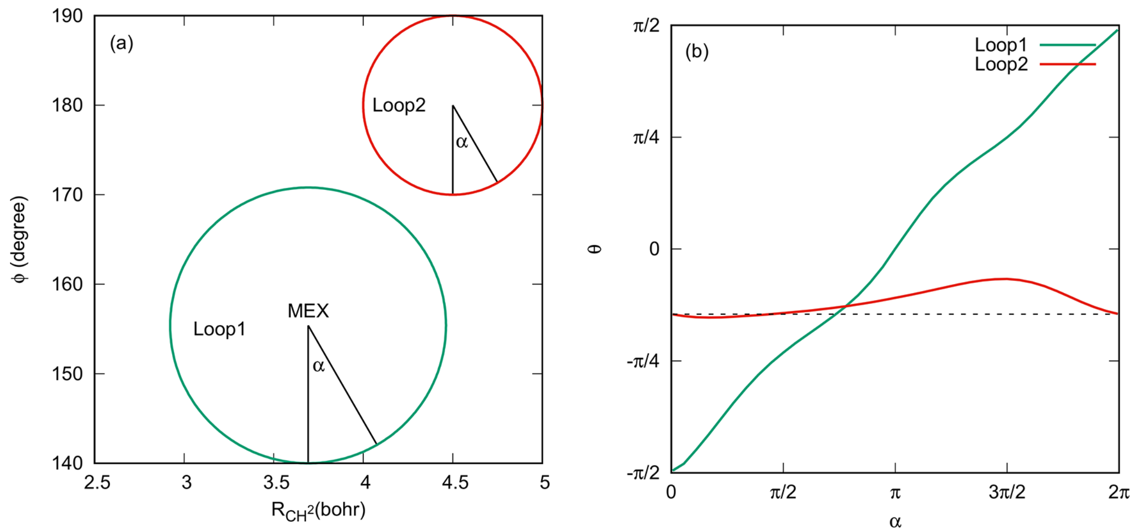

Figure 3. (a) Two closed circular paths in the two-dimensional space, Loop1 and Loop2, are shown. The center of Loop1 is the MEX and the center of Loop2 is the point ($R(CH^2)$ = 4.5 bohr, ϕ = 180°). (b) Rotation angle θ on the closed loops as a function of polar angle α, which is defined as the counterclockwise angle from the vertical axis.

To illustrate that the discontinuities in adiabatic SOCs can be removed through diabatization, an analysis of the SOCs of formaldehyde in a two-dimensional subspace of nuclear coordinate is performed. The two-dimensional space used here has its origin at the minimum energy conical intersection (MEX) between S_0 and S_1, which is shown in Figure 1. The geometry of the MEX was optimized by the COLUMBUS program using multireference configuration interaction (MRCI) with all single- and double-excitation wave functions.[60,61] The COLUMBUS program provides analytical MRCI gradients and derivative couplings, which makes it convenient to locate the MEX. The molecular orbitals are obtained from a state-averaged multiconfiguration self-consistent field treatment that averages two singlet states and one triplet state with equal weights and a full valence active space (10 electrons, 9 orbitals). The basis set used is cc-pVTZ. As can be seen in Figure 1, the CH^2 distance at the MEX is rather large (3.692 bohr), forming a quasiradical structure. Direct dissociation through this conical intersection explains the radical products as produced through internal conversion from S_1 to S_0 via the conical intersection.

The two-dimensional space under study is spanned by $R(CH^2)$ and the out of plane angle ϕ between $\mathbf{R}_{CH^2}$ and $\mathbf{R}_{CO} \times \mathbf{R}_{CH^1}$. A 31 × 11 uniform grid was employed, and the adiabatic energies, dipole moments, transition dipole moments, and SOCs on the grid were calculated from MRCI wave functions with the MOLPRO 2012.1 package.[62] The only difference between the COLUMBUS and MOLPRO calculations is that COLUMBUS program provides an uncontracted MRCI (uc-MRCI), while MOLPRO uses an internally contracted MRCI (ic-MRCI). This difference gives rise to a

https://dx.doi.org/10.1021/acs.jpclett.0c00074
J. Phys. Chem. Lett. 2020, 11, 1848−1858

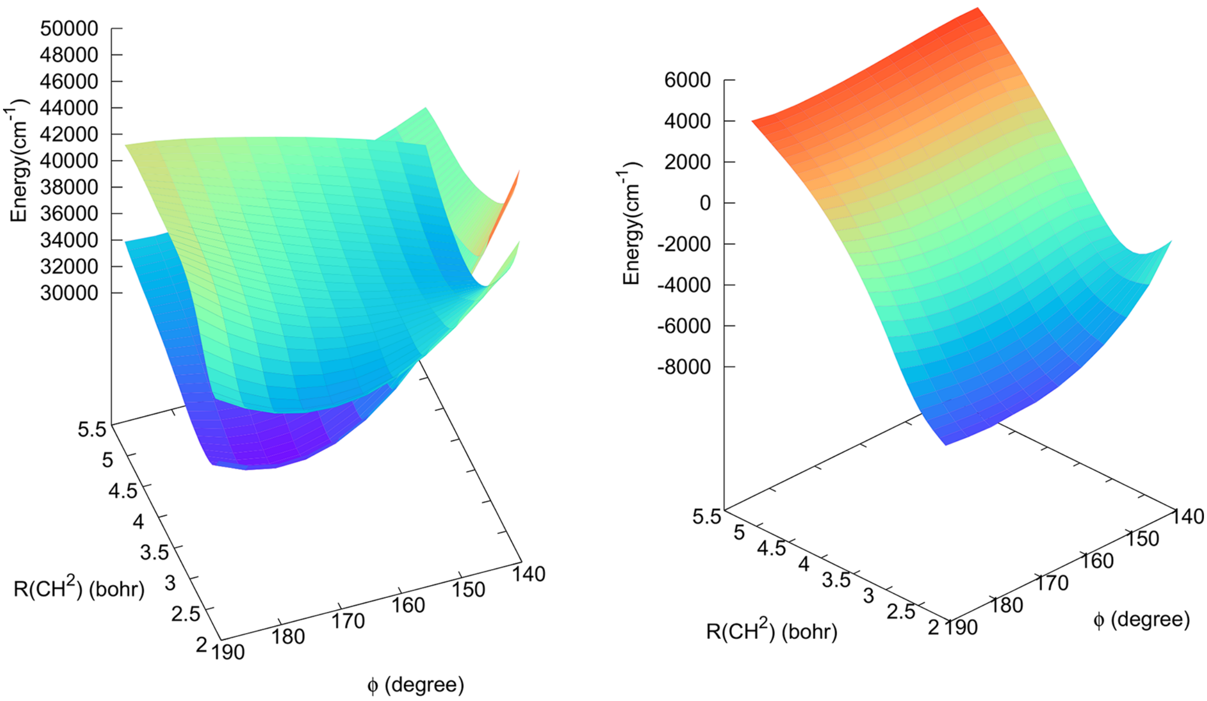

Figure 4. $H_{11}^{(d)}$, $H_{22}^{(d)}$ (left panel), and $H_{12}^{(d)}$ (right panel) in the two-dimensional space.

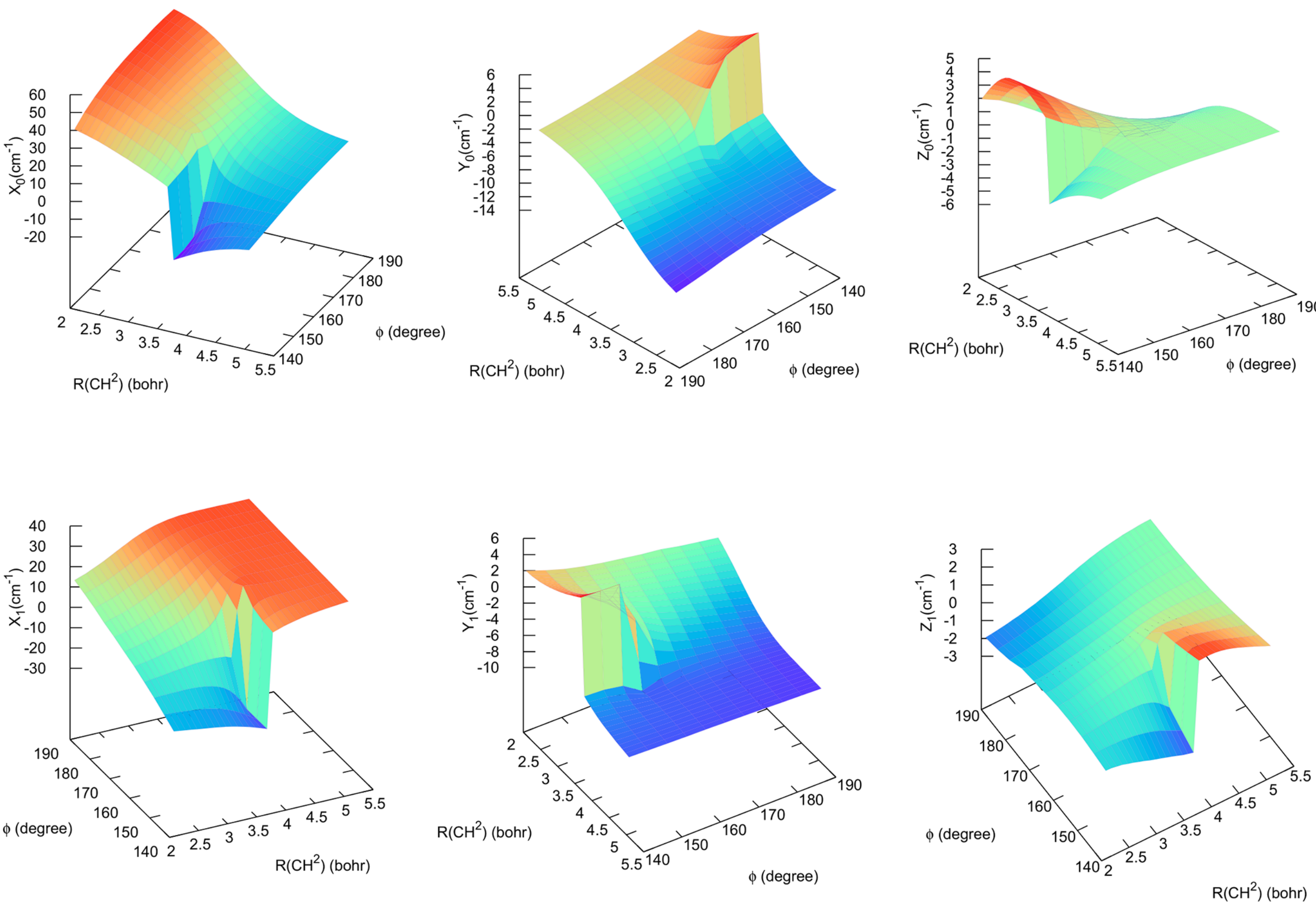

Figure 5. Adiabatic spin−orbit couplings X_0, Y_0, and Z_0 (upper panel) and X_1, Y_1, and Z_1 (lower panel) in the two-dimensional space.

nonzero energy difference of 123 cm^{-1} predicted by MOLPRO at the MEX optimized by COLUMBUS. However, considering the high energy of MEX (∼36 000 cm^{-1}) relative to the energy minimum of formaldehyde on S_0 surface, this difference is rather small, indicating that the MEX optimized by COLUMBUS is very near to that on the MOLPRO surface.

https://dx.doi.org/10.1021/acs.jpclett.0c00074
J. Phys. Chem. Lett. 2020, 11, 1848−1858

Figure 1 shows the adiabatic PESs for S_0, S_1 (left panel), and T_1 (right panel) in the two-dimensional space. A conical intersection between S_0 and S_1 can be observed. Except for this conical intersection, no sign of other intersections is evident on any of the three surfaces, which indicates that at least in this case, S_0, S_1, and T_1 span a *clean* subspace of electronic states for diabatization.[63] By using eq 5 with a large enough weight ($w = 8$ au),[50] the rotation angle θ in the two-dimensional space is obtained as shown in Figure 2. Discontinuities in θ can be observed around MEX ($R(\mathrm{CH}^2) = 3.692$ bohr, $\phi = 155.4°$). These discontinuities are not wrong but rather manifestations of the geometric phase effect (GPE). The GPE can be examined by investigating the changes in rotation angle along closed paths. In panel (a) of Figure 3, two closed circular paths in the two-dimensional space, Loop1 and Loop2, are shown. The center of Loop1 is the MEX, and the center of Loop2 is the point ($R(\mathrm{CH}^2) = 4.5$ bohr, $\phi = 180°$). Loop1 circles the MEX, while Loop2 does not. Panel (b) of Figure 3 then shows the corresponding rotation angle along these two paths as a function of polar angle α, which is defined as the counterclockwise angle from the vertical axis. Along Loop1, rotation angle θ accumulates a change of π. On the other hand, along Loop2, the change in θ is zero, as indicated by the dashed horizontal line. These results are consistent with the GPE. Correspondingly, the diabatic matrix elements $H_{11}^{(d)}$, $H_{22}^{(d)}$, and $H_{12}^{(d)}$ are shown in Figure 4. They all are smooth and continuous functions of nuclear coordinates, which also indicates the validity of the modified BL diabatization.

With a valid diabatization in hand, we are in a position to investigate the SOCs in the adiabatic and diabatic representations. It was mentioned before that the rotational transformation property of SOCs (X_i, Y_i, Z_i) is the same as that of the angular momentum (L_x, L_y, L_z), which is a pseudovector. In order to illustrate the SOCs more clearly, each geometry is placed at its standard orientation to remove the translational and rotational degrees of freedom. The standard orientation used here also defines a body-fixed Cartesian frame. The unit vectors for the body-fixed frame are denoted as $\mathbf{e}_x$, $\mathbf{e}_y$, and $\mathbf{e}_z$. This body-fixed frame is constructed as follows. With the carbon nucleus taken as the origin, the oxygen nucleus is placed on the positive x axis. The positive z axis is set to be along the direction of $\mathbf{R}_{\mathrm{CO}} \times \mathbf{R}_{\mathrm{CH}^1}$, and $\mathbf{e}_y$ is the cross product of $\mathbf{e}_z$ and $\mathbf{e}_x$.

Figure 5 shows the adiabatic SOCs X_0, Y_0, Z_0, X_1, Y_1, and Z_1 in the two-dimensional space described above. As can be seen, the magnitude of SOCs is less than 60 cm^{-1}, which is 2 orders of magnitude smaller than $H_{12}^{(d)}$. This means that compared to internal conversion, intersystem crossing may contribute very little to the direct dissociation of formaldehyde. However, there are other factors to consider. Table 3 lists adiabatic energies of selected critical points of formaldehyde, which include the energy minimum of S_1 (S1min), the saddle point on S_1 (S1sadd) connecting S1min and H + HCO products, the energy minimum of T_1 (T1min), the saddle point on T_1 (T1sadd) connecting T1min and H + HCO products, the minimum energy crossing point between S_0 and S_1 (MEX), the minimum intersystem crossing point between S_0 and T_1 (MSXS0T1), and the minimum intersystem crossing point between S_1 and T_1 (MSXS1T1). These critical points were optimized with COLUMBUS, and the energies shown in the table are relative to the global minimum on S_0. Ab initio calculations indicate that PESs for S_1 and T_1 are parallel to each other over a wide range of configuration space and cross at geometries with extended CO bonds at very high energies. For example, MSXS1T1 has a relatively high energy of 45 162.4 cm^{-1} and a large CO bond distance of 3.50 bohr. Considering the small energy gap between S_1 and T_1 in these regions (around 3000 cm^{-1} at S1min, S1sadd, and T1min), if the excitation energy of the system is not sufficient to overcome the barrier on S_1, less than 37 000 cm^{-1} for example, the system will wander around S1min, and the population on T_1 can accumulate in a long time scale via intersystem crossing between S_1 and T_1 despite the small spin−orbit coupling between them. Then, through the intersystem crossing between S_0 and T_1, products on S_0 can still be obtained.[38] In this regard, note that long time dynamics simulations are not practical with most on-the-fly methods but can be easily performed provided analytical surfaces have been constructed.

Table 3. Adiabatic Energies (cm^{-1}) of Selected Critical Points of Formaldehyde

	$E(S_0)$	$E(S_1)$	$E(T_1)$
S1min	6910.2	28 874.4	26 029.0
S1sadd	30 699.3	37 976.4	35 110.9
T1min	7455.4	28 997.8	25 910.7
T1sadd	28 656.3	40 105.6	34 333.0
MEX	36 163.3	36 163.3	35 328.0
MSXS0T1	33 790.4	39 142.7	33 790.4
MSXS1T1	38 583.1	45 162.4	45 162.4

We now turn to the key issues in this work: the construction of a quasidiabatic representation of all the SOC interactions and their representation by NNs. As can be seen in Figure 5, in the adiabatic representation, all SOC components have obvious discontinuities around MEX. These discontinuities cannot be fit; therefore, a smooth and continuous analytic representation for adiabatic SOCs is not possible. Clearly, an AtD transformation is called for. However, as we will show below, care must be exercised, since one cannot choose the diabatization arbitrarily. A pointwise accurate diabatization should be used, by which we mean a diabatization for which the singularity in the spin−orbit coupling (located at $\mathbf{R}^{\mathrm{SO}}$) is located at the same $\mathbf{R}$ where the derivative coupling is singular (at $\mathbf{R}^{\mathrm{CI}}$). The following observations are germane. (i) In the absence of a pointwise diabatization, the singularity in the SOC will not be completely removed, and the region encompassing $\mathbf{R}^{\mathrm{SO}}$ and $\mathbf{R}^{\mathrm{CI}}$ will require special treatment. (ii) The fit of the diabatization must be performed after the diabatization is used to remove the SOC singularity. (iii) A single conical intersection creates singularities in many SOC terms with dramatically different magnitudes (see Figure 5). One must consider whether the AtD transformation and SOC data are sufficiently accurate to provide meaningful results for all the interactions. (iv) Finally, since all spin orbit diabatic matrix elements originate from adiabatic matrix elements and are expressed as $\langle \mathbf{U}^S(\mathbf{R})\mathbf{\Psi}^{(a),S,M_S}(\mathbf{r};\mathbf{R})|\hat{H}_{\mathrm{SO}}|\mathbf{U}^{S'}(\mathbf{R})\mathbf{\Psi}^{(a),S',M_{S'}}(\mathbf{r};\mathbf{R})\rangle$, where $\mathbf{U}^S$ and $\mathbf{U}^{S'}$ are AtD transformations, several distinct diabatizations can be applied simultaneously.

First, let us examine the adiabatic and diabatized SOCs along Loop1 in Figure 6, where the range of polar angle α is adjusted to $[-\pi, \pi]$, $X_0^{(d)} = H_{13}^{(d)}$, $Y_0^{(d)} = H_{14}^{(d)}$, $Z_0^{(d)} = H_{15}^{(d)}$, $X_1^{(d)} = H_{23}^{(d)}$, $Y_1^{(d)} = H_{24}^{(d)}$, and $Z_1^{(d)} = H_{25}^{(d)}$. As can be seen, all adiabatic SOC matrix elements (upper row) exhibit a discontinuity at $\alpha = 0$. However, after the AtD transformation, the discontinuities disappear, and the resultant diabatized SOCs (lower row) become smooth and continuous functions of nuclear coordinates. Figure 7 provides a

https://dx.doi.org/10.1021/acs.jpclett.0c00074
J. Phys. Chem. Lett. 2020, 11, 1848−1858

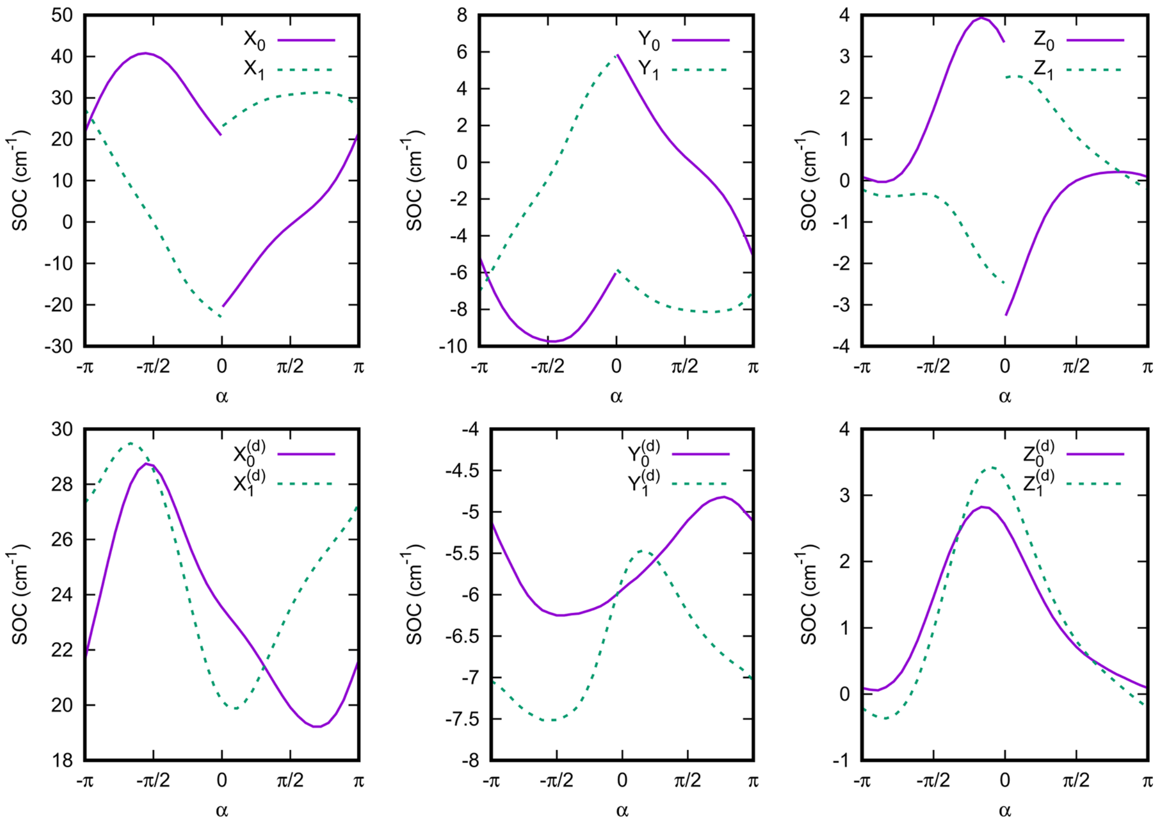

Figure 6. Adiabatic (upper row) and diabatized (lower row) SOCs along Loop1. The range of α is adjusted to $[-\pi, \pi]$.

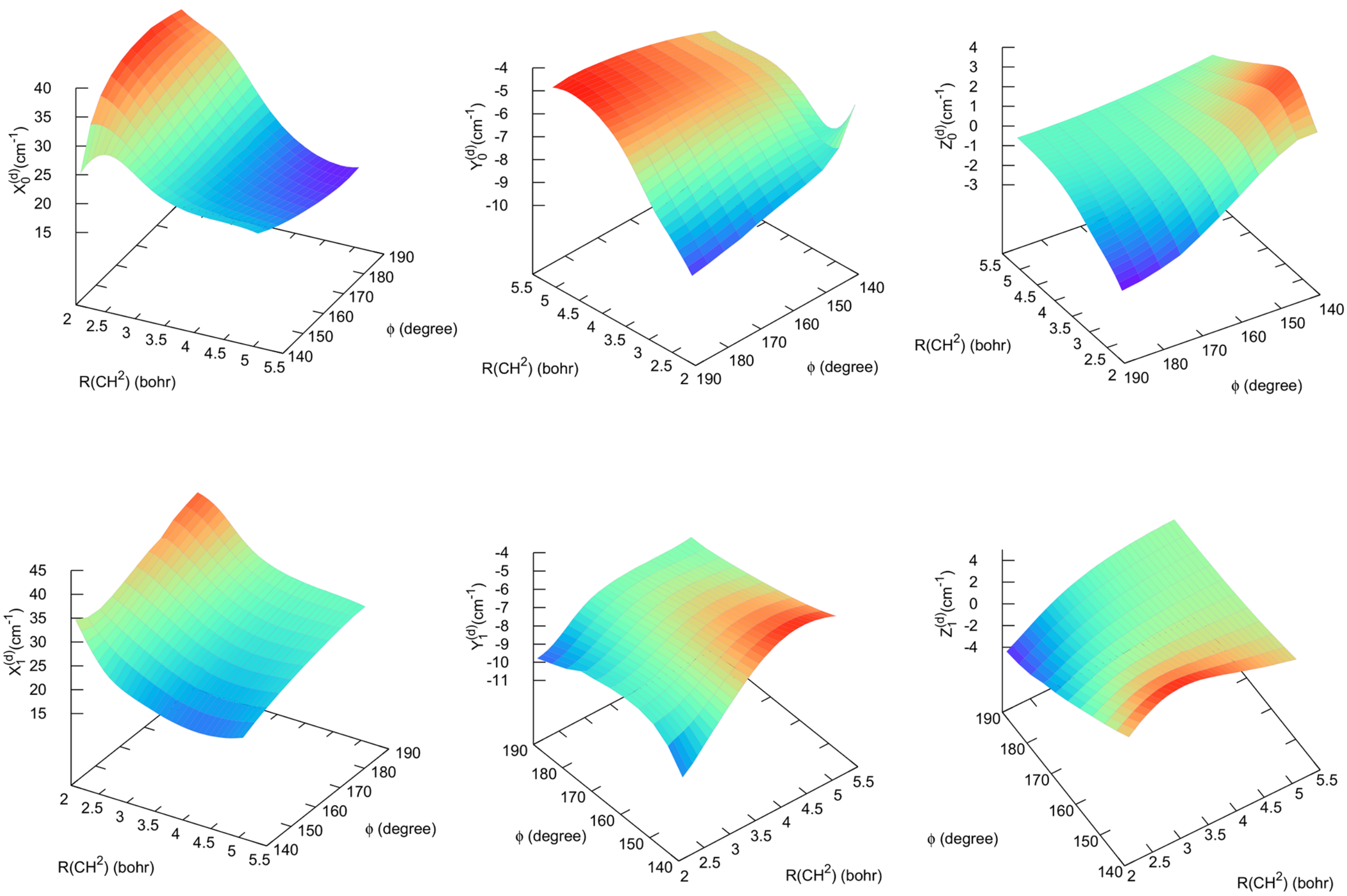

Figure 7. Diabatized spin−orbit couplings $X_0^{(d)}$, $Y_0^{(d)}$, and $Z_0^{(d)}$ (upper panel) and $X_1^{(d)}$, $Y_1^{(d)}$, and $Z_1^{(d)}$ (lower panel) in the two-dimensional space.

https://dx.doi.org/10.1021/acs.jpclett.0c00074
J. Phys. Chem. Lett. 2020, 11, 1848−1858

Table 4. NN Fitting Results with Smallest RMSEs (cm^{-1}) for Each Diabatized Spin−Orbit Coupling Matrix Element[a]

no.	RMSE($X_0^{(d)}$)	RMSE($Y_0^{(d)}$)	RMSE($Z_0^{(d)}$)	RMSE($X_1^{(d)}$)	RMSE($Y_1^{(d)}$)	RMSE($Z_1^{(d)}$)
1	0.0199 (0.088%)	0.0071 (0.142%)	0.0041 (0.064%)	0.0293 (0.133%)	0.0073 (0.151%)	0.0091 (0.108%)
2	0.0199 (0.088%)	0.0071 (0.142%)	0.0042 (0.065%)	0.0297 (0.134%)	0.0073 (0.151%)	0.0093 (0.110%)
3	0.0201 (0.089%)	0.0071 (0.142%)	0.0043 (0.067%)	0.0298 (0.135%)	0.0078 (0.161%)	0.0096 (0.113%)
4	0.0202 (0.090%)	0.0072 (0.144%)	0.0043 (0.067%)	0.0318 (0.144%)	0.0084 (0.174%)	0.0096 (0.113%)
5	0.0202 (0.090%)	0.0072 (0.144%)	0.0044 (0.069%)	0.0323 (0.146%)	0.0089 (0.184%)	0.0097 (0.115%)
6	0.0203 (0.090%)	0.0072 (0.144%)	0.0044 (0.069%)	0.0325 (0.147%)	0.0092 (0.190%)	0.0097 (0.115%)
7	0.0203 (0.090%)	0.0072 (0.144%)	0.0044 (0.069%)	0.0328 (0.149%)	0.0094 (0.194%)	0.0098 (0.116%)
8	0.0205 (0.091%)	0.0072 (0.144%)	0.0044 (0.069%)	0.0331 (0.150%)	0.0094 (0.194%)	0.0098 (0.116%)
9	0.0206 (0.091%)	0.0072 (0.144%)	0.0045 (0.070%)	0.0336 (0.152%)	0.0095 (0.196%)	0.0098 (0.116%)
10	0.0207 (0.092%)	0.0072 (0.144%)	0.0045 (0.070%)	0.0338 (0.153%)	0.0095 (0.196%)	0.0100 (0.118%)
final	0.0197 (0.087%)	0.0070 (0.140%)	0.0042 (0.065%)	0.0300 (0.136%)	0.0078 (0.161%)	0.0093 (0.110%)

[a]The corresponding NRMSEs are listed in parentheses.

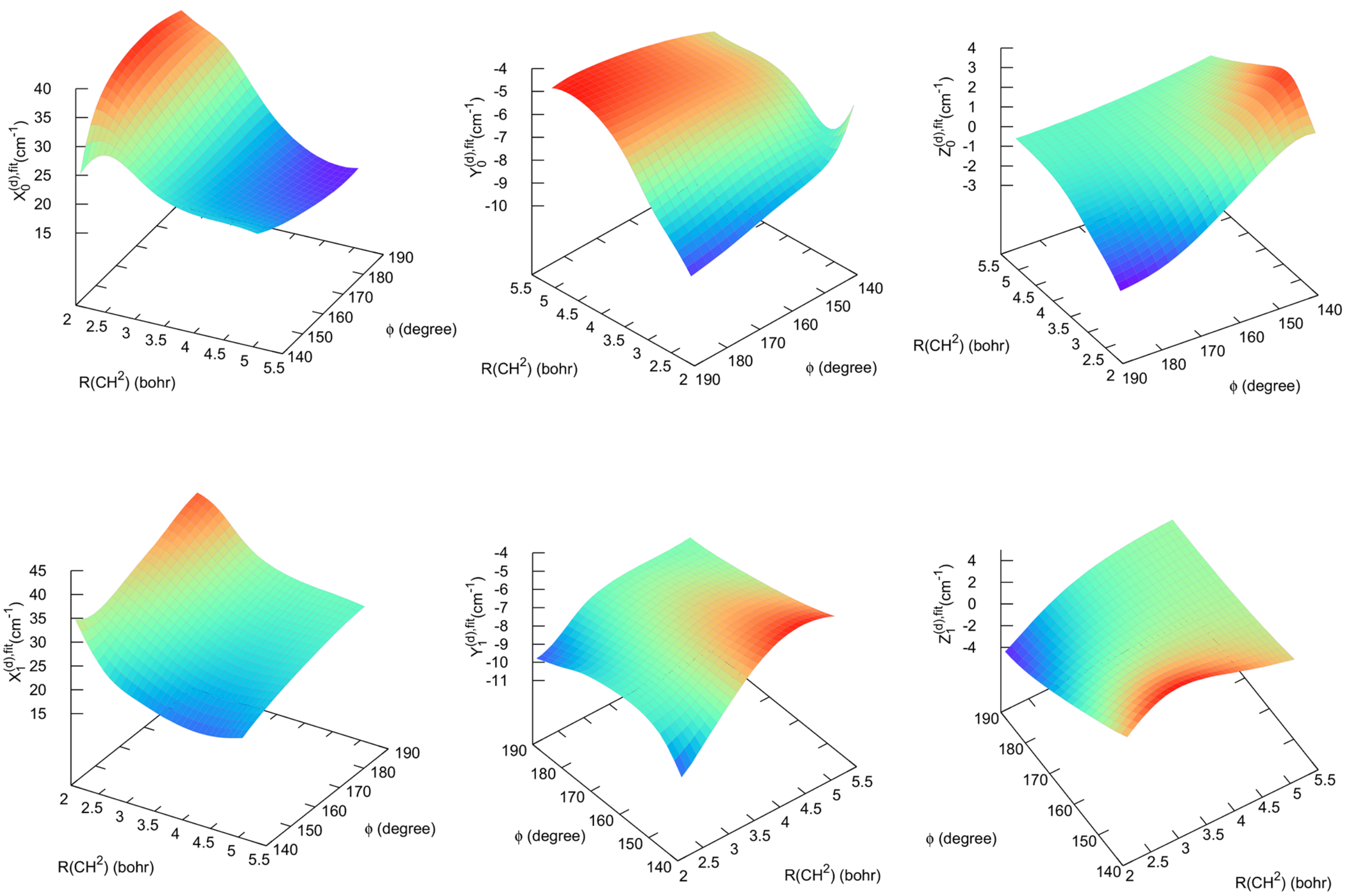

Figure 8. NN fitted diabatized spin−orbit couplings $X_0^{(d),\mathrm{fit}}$, $Y_0^{(d),\mathrm{fit}}$, and $Z_0^{(d),\mathrm{fit}}$ (upper panel) and $X_1^{(d),\mathrm{fit}}$, $Y_1^{(d),\mathrm{fit}}$, and $Z_1^{(d),\mathrm{fit}}$ (lower panel) in the two-dimensional space.

global view of diabatized SOCs in the two-dimensional space, where the smoothness of the diabatized SOCs is evident. It is important to note that the relative phases of the S_0, S_1, and T_1 wave functions in ab initio calculations have been manually adjusted to obtain smooth diabatized spin−orbit couplings.

To further demonstrate the smooth and continuous character of the diabatized SOCs, they will be represented by analytical functions. In this work, feed-forward NNs are employed to fit the diabatized spin−orbit couplings. The structure and definition of the feed-forward NN can be found elsewhere.[31] To fit each spin−orbit coupling matrix element, a feed-forward NN with structure 2−10−10−1 is used, which means that this NN takes $R(\mathrm{CH}^2)$ and ϕ as input, has two hidden layers, both of which have 10 neurons, and gives a scalar output. The transfer function in the first and second layers is a hyperbolic tangent function $f(x) = \tanh(x)$; in the third layer, it is a linear function $f(x) = x$. The training of an NN produces optimized NN parameters $\boldsymbol{\lambda}$ by minimizing the following performance index

$$P(\boldsymbol{\lambda}) = \frac{1}{2}\sum_{q=1}^{Q}(X_q^{(d)} - X_q^{(d),\mathrm{fit}})^2 \tag{7}$$

where Q is the number of data points, $X_q^{(d)}$ is the qth data point of diabatized spin−orbit coupling matrix element $X^{(d)}$, and $X_q^{(d),\mathrm{fit}}$ is the corresponding NN prediction for qth data point. The Levenberg−Marquart algorithm is used to minimize the

https://dx.doi.org/10.1021/acs.jpclett.0c00074
J. Phys. Chem. Lett. 2020, 11, 1848−1858

performance index. It is very numerically robust and can achieve convergence very quickly.[64] For each spin−orbit coupling matrix element, a total of 341 data points were assembled. Before fitting, the data were normalized linearly to fall into a standard range [−1,1]. In each training, all the data points were randomly divided into training set (90%) and validation set (10%), and an early stopping method was employed to avoid over fitting, where training is stopped if the error on the validation set goes up for several iterations.[65] In order to achieve the best results, 50 trainings with different initial parameters were performed, from which the fittings with smallest root-mean-square error on the whole data set were selected as the optimal results. The definition of root-mean-square error is

$$\mathrm{RMSE}(X^{(d)}) = \sqrt{\frac{\sum_{q=1}^{Q} (X_q^{(d)} - X_q^{(d),\mathrm{fit}})^2}{Q}} \tag{8}$$

Table 4 lists 10 fitting results with the smallest RMSEs for each diabatized SOC matrix element. The corresponding normalized root-mean-square error (NRMSE) for each diabatized SOC matrix element is also listed in parentheses. The NRMSE is defined as

$$\mathrm{NRMSE}(X^{(d)}) = \frac{\mathrm{RMSE}(X^{(d)})}{\max(X^{(d)}) - \min(X^{(d)})} \tag{9}$$

The NRMSE facilitates comparison of the fitting results for different diabatized SOC matrix elements, which have different scales. As can be seen in Table 4, the NRMSEs are very small, showing that NNs can accurately reproduce the fitting data. The NRMSEs of different diabatized SOC matrix elements are of similar magnitude, which is expected since the fitting data have been normalized before fitting. The SOC matrix elements that have larger magnitude will then have larger RMSEs, which explains the larger RMSEs for $X_0^{(d)}$ and $X_1^{(d)}$ when compared to those for the $Y^{(d)}$ and $Z^{(d)}$ counterparts. The final NN result for each diabatized spin−orbit coupling matrix element is chosen as the average of the 10 fits with the smallest RMSEs. By averaging multiple results, more accurate results can be obtained.[66−68] The RMSEs (NRMSEs) for final results are also listed in Table 4. Figure 8 presents the NN fitted SOC matrix elements in the two-dimensional space. None of the NN fitted elements show any sign of oscillations. The NN model can interpolate very well between data points, and the smoothness is thus evident.

In summary, in this work, we have demonstrated that another molecular interaction spin−orbit coupling can be diabatized and fit with artificial neural networks. This will allow the fit-coupled-surface method in the diabatic representation to be used to study the competition between internal conversion and intersystem crossing very accurately. The singlet-states S_0 and S_1 and a triplet T_1 state of formaldehyde were studied as a test example. The spin−orbit couplings between S_0, S_1, and triplet T_1 were analyzed in a two-dimensional subspace of nuclear coordinate space. First, a modified Boys localization diabatization method was employed to diabatize S_0 and S_1. It generates a proper diabatic representation that can remove singular derivative couplings at conical intersections and is free from the unphysical diabolical singularities. Then the spin−orbit couplings were transformed to the diabatic representation. In the diabatic representation, the discontinuities in spin−orbit couplings around a conical intersection are removed, and the resultant diabatized spin−orbit couplings become smooth and continuous functions of nuclear coordinates. Finally, the diabatized spin−orbit couplings were accurately fit by smooth and continuous neural network functions, which serve to confirm the smoothness and continuity of the representation and is of practical utility.

Thus, this work provides an initial example of a robust procedure for fitting spin−orbit couplings obtained initially in the convenient adiabatic eigenstate representation using a standard diabatic representation and neural networks and demonstrates that an analytic representation of spin−orbit couplings is possible despite the presence of conical intersections. To fully study the competition between internal conversion and intersystem crossing in the photodissociation of formaldehyde, a subject with a long history,[69] a global description is indispensable. This is the direction to be pursued in our future work. In that work, the domain of the $\mathbf{H}^{(d)}$ will be extended to all dynamically relevant regions, using the trajectory-guided point sampling approach.[15] Another important issue to be addressed in that work is how to remove the arbitrariness in the phases (signs) of electronic wave functions in ab initio calculations. This arbitrariness leaves the signs of transition dipole moments between S_0 and S_1 and the spin−orbit couplings between singlet states and triplet state undetermined. In this work, the signs of transition dipole moments, the value of k in eq 6, and the signs of spin−orbit couplings have been manually adjusted to achieve smoothness in $\mathbf{H}^{(d)}$. Based on the smooth $\mathbf{H}^{(d)}$ in the two-dimensional subspace used in this work, the sign consistency can be achieved globally by a cluster growing algorithm, the success of which has been reported previously.[7,21] Finally the global $\mathbf{H}^{(d)}$ can be fit with neural networks.

With this fit accomplished, we will have constructed a fit diabatic representation based on high quality ab initio data of the diabatic potential energy matrix, the dipole and transition dipole moments, and the spin−orbit interaction for S_0, S_1, and T_1 using neural networks. Considering the low number of nuclear degrees of freedom (6) in formaldehyde, full-dimensional quantum dynamics simulations will be feasible, enabling treatments of photodissociation of unprecedented accuracy.

■ ASSOCIATED CONTENT

Supporting Information

The Supporting Information is available free of charge at https://pubs.acs.org/doi/10.1021/acs.jpclett.0c00074.

Symmetry analysis of the adiabatic SOCs for formaldehyde (PDF); the codes, fitting data, and details of neural networks fitting are attached (CODE) (ZIP)

■ AUTHOR INFORMATION

Corresponding Authors

Yafu Guan − *Department of Chemistry, Johns Hopkins University, Baltimore, Maryland 21218, United States*; Email: yguan15@jhu.edu

David R. Yarkony − *Department of Chemistry, Johns Hopkins University, Baltimore, Maryland 21218, United States*; orcid.org/0000-0002-5446-1350; Email: yarkony@jhu.edu

Complete contact information is available at: https://pubs.acs.org/10.1021/acs.jpclett.0c00074

Notes

The authors declare no competing financial interest.

https://dx.doi.org/10.1021/acs.jpclett.0c00074
J. Phys. Chem. Lett. 2020, 11, 1848−1858

■ ACKNOWLEDGMENTS

This work is supported by National Science Foundation grant CHE 1663692 to D.R.Y. The authors acknowledge a generous grant of computer time from the Maryland Advanced Research Computing Center (MARCC) and from the National Energy Research Scientific Computing Center (NERSC).

■ REFERENCES

(1) Marian, C. M. Spin−orbit coupling and intersystem crossing in molecules. *WIREs Comput. Mol. Sci.* **2012**, *2*, 187−203.
(2) Curchod, B. F. E.; Rauer, C.; Marquetand, P.; González, L.; Martínez, T. J. Communication: GAIMS—Generalized Ab Initio Multiple Spawning for both internal conversion and intersystem crossing processes. *J. Chem. Phys.* **2016**, *144*, 101102.
(3) Mai, S.; Marquetand, P.; González, L. A general method to describe intersystem crossing dynamics in trajectory surface hopping. *Int. J. Quantum Chem.* **2015**, *115*, 1215−1231.
(4) Mai, S.; Marquetand, P.; González, L. Nonadiabatic dynamics: The SHARC approach. *Wiley Interdiscip. Rev. Comput. Mol. Sci.* **2018**, *8*, e1370.
(5) Richings, G. W.; Habershon, S. Direct grid-based quantum dynamics on propagated diabatic potential energy surfaces. *Chem. Phys. Lett.* **2017**, *683*, 228−233.
(6) Zhu, X.; Yarkony, D. R. Fitting coupled potential energy surfaces for large systems: Method and construction of a 3-state representation for phenol photodissociation in the full 33 internal degrees of freedom using multireference configuration interaction determined data. *J. Chem. Phys.* **2014**, *140*, 024112.
(7) Guan, Y.; Guo, H.; Yarkony, D. R. Extending the Representation of Multistate Coupled Potential Energy Surfaces To Include Properties Operators Using Neural Networks: Application to the $1,2^1A$ States of Ammonia. *J. Chem. Theory Comput.* **2020**, *16*, 302−313.
(8) Mai, S.; Atkins, A. J.; Plasser, F.; González, L. The Influence of the Electronic Structure Method on Intersystem Crossing Dynamics. The Case of Thioformaldehyde. *J. Chem. Theory Comput.* **2019**, *15*, 3470−3480.
(9) Westermann, T.; Eisfeld, W.; Manthe, U. Coupled potential energy surface for the $F(^2P) + CH_4 \rightarrow HF + CH_3$ entrance channel and quantum dynamics of the $CH_4{\cdot}F^-$ photodetachment. *J. Chem. Phys.* **2013**, *139*, 014309.
(10) Lenzen, T.; Manthe, U. Vibronically and spin-orbit coupled diabatic potentials for $X(P) + CH_4 \rightarrow HX + CH_3$ reactions: General theory and application for $X(P) = F(^2P)$. *J. Chem. Phys.* **2019**, *150*, 064102.
(11) Baer, M. Adiabatic and diabatic representations for atom-diatom collisions: Treatment of the three-dimensional case. *Chem. Phys.* **1976**, *15*, 49−57.
(12) Mead, C. A.; Truhlar, D. G. Conditions for the definition of a strictly diabatic electronic basis for molecular systems. *J. Chem. Phys.* **1982**, *77*, 6090−6098.
(13) Baer, M. Introduction to the theory of electronic non-adiabatic coupling terms in molecular systems. *Phys. Rep.* **2002**, *358*, 75−142.
(14) Zhu, X.; Yarkony, D. R. Toward eliminating the electronic structure bottleneck in nonadiabatic dynamics on the fly: An algorithm to fit nonlocal, quasidiabatic, coupled electronic state Hamiltonians based on ab initio electronic structure data. *J. Chem. Phys.* **2010**, *132*, 104101.
(15) Zhu, X.; Yarkony, D. R. On the representation of coupled adiabatic potential energy surfaces using quasi-diabatic Hamiltonians: A distributed origins expansion approach. *J. Chem. Phys.* **2012**, *136*, 174110.
(16) Zhu, X.; Yarkony, D. R. Quasi-diabatic representations of adiabatic potential energy surfaces coupled by conical intersections including bond breaking: A more general construction procedure and an analysis of the diabatic representation. *J. Chem. Phys.* **2012**, *137*, 22A511.
(17) Ma, J.; Zhu, X.; Guo, H.; Yarkony, D. R. First principles determination of the $NH_2/ND_2(\tilde{A}/\tilde{X})$ branching ratios for photodissociation of NH_3/ND_3 via full-dimensional quantum dynamics based on a new quasi-diabatic representation of coupled ab initio potential energy surfaces. *J. Chem. Phys.* **2012**, *137*, 22A541.
(18) Ma, J.; Xie, C.; Zhu, X.; Yarkony, D. R.; Xie, D.; Guo, H. Full-Dimensional Quantum Dynamics of Vibrationally Mediated Photodissociation of NH_3 and ND_3 on Coupled Ab Initio Potential Energy Surfaces: Absorption Spectra and $NH_2(\tilde{A}^2A_1)/NH_2(\tilde{X}^2B_1)$ Branching Ratios. *J. Phys. Chem. A* **2014**, *118*, 11926−11934.
(19) Xie, C.; Ma, J.; Zhu, X.; Zhang, D. H.; Yarkony, D. R.; Xie, D.; Guo, H. Full-Dimensional Quantum State-to-State Nonadiabatic Dynamics for Photodissociation of Ammonia in its A-Band. *J. Phys. Chem. Lett.* **2014**, *5*, 1055−1060.
(20) Xie, C.; Zhu, X.; Ma, J.; Yarkony, D. R.; Xie, D.; Guo, H. Communication: On the competition between adiabatic and nonadiabatic dynamics in vibrationally mediated ammonia photodissociation in its A band. *J. Chem. Phys.* **2015**, *142*, 091101.
(21) Shu, Y.; Kryven, J.; Sampaio de Oliveira-Filho, A. G.; Zhang, L.; Song, G.-L.; Li, S. L.; Meana-Pañeda, R.; Fu, B.; Bowman, J. M.; Truhlar, D. G. Direct Diabatization and Analytic Representation of Coupled Potential Energy Surfaces and Couplings for the Reactive Quenching of the Excited $^2\Sigma^+$ State of OH by Molecular Hydrogen. *J. Chem. Phys.* **2019**, *151*, 104311.
(22) Williams, C. K.; Rasmussen, C. E. *Gaussian processes for machine learning*; MIT Press: Cambridge, MA, 2006; Vol. *2*.
(23) Ndome, H.; Welsch, R.; Eisfeld, W. A new method to generate spin-orbit coupled potential energy surfaces: Effective relativistic coupling by asymptotic representation. *J. Chem. Phys.* **2012**, *136*, 034103.
(24) Zeng, T. A diabatization protocol that includes spin-orbit coupling. *J. Chem. Phys.* **2017**, *146*, 144103.
(25) Lévêque, C.; Taïeb, R.; Köppel, H. Communication: Theoretical prediction of the importance of the $^3B_2$ state in the dynamics of sulfur dioxide. *J. Chem. Phys.* **2014**, *140*, 091101.
(26) Westermayr, J.; Gastegger, M.; Menger, M. F. S. J.; Mai, S.; González, L.; Marquetand, P. Machine learning enables long time scale molecular photodynamics simulations. *Chem. Sci.* **2019**, *10*, 8100−8107.
(27) Chen, W.-K.; Liu, X.-Y.; Fang, W.-H.; Dral, P. O.; Cui, G. Deep Learning for Nonadiabatic Excited-State Dynamics. *J. Phys. Chem. Lett.* **2018**, *9*, 6702−6708.
(28) Richings, G. W.; Robertson, C.; Habershon, S. Improved on-the-Fly MCTDH Simulations with Many-Body-Potential Tensor Decomposition and Projection Diabatization. *J. Chem. Theory Comput.* **2019**, *15*, 857−870.
(29) Polyak, I.; Richings, G. W.; Habershon, S.; Knowles, P. J. Direct quantum dynamics using variational Gaussian wavepackets and Gaussian process regression. *J. Chem. Phys.* **2019**, *150*, 041101.
(30) Xie, C.; Zhu, X.; Yarkony, D. R.; Guo, H. Permutation invariant polynomial neural network approach to fitting potential energy surfaces. IV. Coupled diabatic potential energy matrices. *J. Chem. Phys.* **2018**, *149*, 144107.
(31) Guan, Y.; Zhang, D. H.; Guo, H.; Yarkony, D. R. Representation of coupled adiabatic potential energy surfaces using neural network based quasi-diabatic Hamiltonians: $1,2\ ^2A'$ states of LiFH. *Phys. Chem. Chem. Phys.* **2019**, *21*, 14205−14213.
(32) Guan, Y.; Guo, H.; Yarkony, D. R. Neural network based quasi-diabatic Hamiltonians with symmetry adaptation and a correct description of conical intersections. *J. Chem. Phys.* **2019**, *150*, 214101.
(33) Carbogno, C.; Behler, J.; Reuter, K.; Groß, A. Signatures of nonadiabatic O_2 dissociation at Al(111): First-principles fewest-switches study. *Phys. Rev. B: Condens. Matter Mater. Phys.* **2010**, *81*, 035410.
(34) Moore, C. B.; Weisshaar, J. C. Formaldehyde Photochemistry. *Annu. Rev. Phys. Chem.* **1983**, *34*, 525−555.
(35) Yates, B. F.; Yamaguchi, Y.; Schaefer, H. F. The dissociation mechanism of triplet formaldehyde. *J. Chem. Phys.* **1990**, *93*, 8798−8807.
(36) Townsend, D.; Lahankar, S. A.; Lee, S. K.; Chambreau, S. D.; Suits, A. G.; Zhang, X.; Rheinecker, J.; Harding, L. B.; Bowman, J. M.

The Roaming Atom: Straying from the Reaction Path in Formaldehyde Decomposition. *Science* **2004**, *306*, 1158−1161.

(37) Araujo, M.; Lasorne, B.; Bearpark, M. J.; Robb, M. A. The Photochemistry of Formaldehyde: Internal Conversion and Molecular Dissociation in a Single Step? *J. Phys. Chem. A* **2008**, *112*, 7489−7491.

(38) Araújo, M.; Lasorne, B.; Magalhães, A. L.; Worth, G. A.; Bearpark, M. J.; Robb, M. A. The molecular dissociation of formaldehyde at medium photoexcitation energies: A quantum chemistry and direct quantum dynamics study. *J. Chem. Phys.* **2009**, *131*, 144301.

(39) Araújo, M.; Lasorne, B.; Magalhães, A. L.; Bearpark, M. J.; Robb, M. A. Controlling Product Selection in the Photodissociation of Formaldehyde: Direct Quantum Dynamics from the S_1 Barrier. *J. Phys. Chem. A* **2010**, *114*, 12016−12020.

(40) Quinn, M. S.; Andrews, D. U.; Nauta, K.; Jordan, M. J. T.; Kable, S. H. The energy dependence of CO(v,J) produced from H_2CO via the transition state, roaming, and triple fragmentation channels. *J. Chem. Phys.* **2017**, *147*, 013935.

(41) Fu, B.; Shepler, B. C.; Bowman, J. M. Three-State Trajectory Surface Hopping Studies of the Photodissociation Dynamics of Formaldehyde on ab Initio Potential Energy Surfaces. *J. Am. Chem. Soc.* **2011**, *133*, 7957−7968.

(42) Zhang, P.; Maeda, S.; Morokuma, K.; Braams, B. J. Photochemical reactions of the low-lying excited states of formaldehyde: T_1/S_0 intersystem crossings, characteristics of the S_1 and T_1 potential energy surfaces, and a global T_1 potential energy surface. *J. Chem. Phys.* **2009**, *130*, 114304.

(43) Maeda, S.; Ohno, K.; Morokuma, K. Automated Global Mapping of Minimal Energy Points on Seams of Crossing by the Anharmonic Downward Distortion Following Method: A Case Study of H_2CO. *J. Phys. Chem. A* **2009**, *113*, 1704−1710.

(44) Bethe, H. A.; Salpeter, E. E. *Quantum mechanics of one-and two-electron atoms*; Springer-Verlag: Berlin, 1957.

(45) Langhoff, S. R.; Kern, C. W. *Applications of Electronic Structure Theory*; Springer, 1977; pp 381−437.

(46) Kryachko, E. S.; Yarkony, D. R. Diabatic bases and molecular properties. *Int. J. Quantum Chem.* **2000**, *76*, 235−243.

(47) Mead, C. A. The "noncrossing" rule for electronic potential energy surfaces: The role of time-reversal invariance. *J. Chem. Phys.* **1979**, *70*, 2276−2283.

(48) Subotnik, J. E.; Yeganeh, S.; Cave, R. J.; Ratner, M. A. Constructing diabatic states from adiabatic states: Extending generalized Mulliken−Hush to multiple charge centers with Boys localization. *J. Chem. Phys.* **2008**, *129*, 244101.

(49) Zhu, X.; Yarkony, D. R. On the Construction of Property Based Diabatizations: Diabolical Singular Points. *J. Phys. Chem. A* **2015**, *119*, 12383−12391.

(50) Zhu, X.; Yarkony, D. R. Constructing diabatic representations using adiabatic and approximate diabatic data − Coping with diabolical singularities. *J. Chem. Phys.* **2016**, *144*, 044104.

(51) Wang, Y.; Yarkony, D. R. Determining whether diabolical singularities limit the accuracy of molecular property based diabatic representations: The $1,2^1A$ states of methylamine. *J. Chem. Phys.* **2018**, *149*, 154108.

(52) Wang, Y.; Guan, Y.; Yarkony, D. R. On the Impact of Singularities in the Two-State Adiabatic to Diabatic State Transformation: A Global Treatment. *J. Phys. Chem. A* **2019**, *123*, 9874−9880.

(53) Berry, M. V. Quantal phase factors accompanying adiabatic changes. *Proc. R. Soc. London A* **1984**, *392*, 45−57.

(54) Ryabinkin, I. G.; Izmaylov, A. F. Geometric Phase Effects in Dynamics Near Conical Intersections: Symmetry Breaking and Spatial Localization. *Phys. Rev. Lett.* **2013**, *111*, 220406.

(55) Izmaylov, A. F. Perturbative wave-packet spawning procedure for non-adiabatic dynamics in diabatic representation. *J. Chem. Phys.* **2013**, *138*, 104115.

(56) Ryabinkin, I. G.; Joubert-Doriol, L.; Izmaylov, A. F. When do we need to account for the geometric phase in excited state dynamics? *J. Chem. Phys.* **2014**, *140*, 214116.

(57) Gherib, R.; Ryabinkin, I. G.; Izmaylov, A. F. Why Do Mixed Quantum-Classical Methods Describe Short-Time Dynamics through Conical Intersections So Well? Analysis of Geometric Phase Effects. *J. Chem. Theory Comput.* **2015**, *11*, 1375−1382.

(58) Gherib, R.; Ye, L.; Ryabinkin, I. G.; Izmaylov, A. F. On the inclusion of the diagonal Born-Oppenheimer correction in surface hopping methods. *J. Chem. Phys.* **2016**, *144*, 154103.

(59) Malbon, C. L.; Zhu, X.; Guo, H.; Yarkony, D. R. On the incorporation of the geometric phase in general single potential energy surface dynamics: A removable approximation to ab initio data. *J. Chem. Phys.* **2016**, *145*, 234111.

(60) Lischka, H.; Shepard, R.; Pitzer, R. M.; Shavitt, I.; Dallos, M.; Müller, T.; Szalay, P. G.; Seth, M.; Kedziora, G. S.; Yabushita, S.; Zhang, Z. High-level multireference methods in the quantum-chemistry program system COLUMBUS: Analytic MR-CISD and MR-AQCC gradients and MR-AQCC-LRT for excited states, GUGA spin−orbit CI and parallel CI density. *Phys. Chem. Chem. Phys.* **2001**, *3*, 664−673.

(61) Lischka, H.; Dallos, M.; Szalay, P. G.; Yarkony, D. R.; Shepard, R. Analytic evaluation of nonadiabatic coupling terms at the MR-CI level. I. Formalism. *J. Chem. Phys.* **2004**, *120*, 7322−7329.

(62) Werner, H.-J.; et al. *MOLPRO, version 2012.1, a package of ab initio programs*; 2012; see http://www.molpro.net.

(63) Baer, M. *Beyond Born-Oppenheimer: electronic nonadiabatic coupling terms and conical intersections*; John Wiley & Sons, 2006.

(64) Hagan, M. T.; Menhaj, M. B. Training feedforward networks with the Marquardt algorithm. *IEEE Transactions on Neural Networks* **1994**, *5*, 989−993.

(65) Sarle, W. S. Stopped Training and Other Remedies for Overfitting. *Proceedings of the 27th Symposium on the Interface of Computing Science and Statistics*; 1995; pp 352−360.

(66) Agrafiotis, D. K.; Cedeño, W.; Lobanov, V. S. On the Use of Neural Network Ensembles in QSAR and QSPR. *J. Chem. Inf. Comput. Sci.* **2002**, *42*, 903−911.

(67) Zhou, Z.; Wu, J.; Tang, W. Ensembling neural networks: Many could be better than all. *Artif. Intell.* **2002**, *137*, 239−263.

(68) Li, J.; Jiang, B.; Guo, H. Permutation invariant polynomial neural network approach to fitting potential energy surfaces. II. Four-atom systems. *J. Chem. Phys.* **2013**, *139*, 204103.

(69) Houston, P. L.; Wang, X.; Ghosh, A.; Bowman, J. M.; Quinn, M. S.; Kable, S. H. Formaldehyde roaming dynamics: Comparison of quasi-classical trajectory calculations and experiments. *J. Chem. Phys.* **2017**, *147*, 013936.

https://dx.doi.org/10.1021/acs.jpclett.0c00074
J. Phys. Chem. Lett. 2020, 11, 1848−1858